

Experimental and numerical investigation of expanded metal tube absorber under axial impact loading

M. Damghani Nouri^a, H. Hatami* and A. Ghodsbin Jahromi^b

Faculty of Mechanical Engineering, Semnan University, Iran

(Received August 21, 2014, Revised December 21, 2014, Accepted May 5, 2015)

Abstract. In this research, the cylindrical absorber made of expanded metal sheets under impact loading has been examined. Expanded metal sheets due to their low weight, effective collapse mechanism has a high energy absorption capacity. Two types of absorbers with different cells angle were examined. First, the absorber with cell angle $\alpha=0$ and then the absorber with angle cell $\alpha=90$. Experimental Study is done by drop Hammer device and numerical investigation is done by finite element of ABAQUS software. The output of device is acceleration-time Diagram which is shown by Accelerometer that is located on the picky mass. Also the output of ABAQUS software is shown by force-displacement diagram. In this research, the numerical and experimental study of the collapse type, force-displacement diagrams and effective parameters has been investigated. Similarly, the comparison between numerical and experimental results has been observed that these results are matched well with each other. From the obtained results it was observed that the absorber with cell angle $\alpha=0$, have symmetric collapse and had high energy absorption capacity but the absorber with cell angle $\alpha=90$, had global buckling and the energy absorption value was not suitable.

Keywords: expanded metal sheet; energy absorption capacity; energy absorbers; dynamic axial loading; impact force; finite element

1. Introduction

Energy absorption systems are used in many engineering applications, moving systems in particular, for preventing or reducing damage. Thin-walled structures are high strength-to-weight ratios and high energy absorption capacity. For this reason, they are the center of attention in many different industries including car manufacturing industries. In some systems, energy absorbers are used for absorbing kinetic energy or converting it into other forms of energy. Mechanical cylindrical tube, absorb energy through doing work in the plastic region. The most common absorbers are thin-walled cylindrical shells which dissipate energy by collapsing under axial loads. These absorbers are irreversible and cannot be reused upon deformation.

Most absorbers are of the throw-away type and are discarded upon plastic deformation. For this

*Corresponding author, Ph.D. Student, E-mail: h64hatami@gmail.com

^aAssociate Professor, E-mail: mnoori@semnan.ac.ir

^bMsc Student, E-mail: ali.ghodsbin.j@gmail.com

reason, design requirements for such tubes would be achieving higher absorbing capability at lower mass with emphasis on higher specific energy absorption. Axial collapse in different designs usually occurs in three stages. First, the collapse force reaches a peak value to overcome the initial tube resistance. Second, the force diminishes and fluctuates as crushing develops. Third, the force rapidly increases, expanding the collapsed parts until the collapse ends. (Ghamarian *et al.* 2011, Jie *et al.* 2013).

Generally, expanded metal tubes are used in the decoration industry and for security purposes. In recent years, expanded metal tubes have found prominent applications in the automobile industry. These materials are specifically used in sensitive structures, e.g., thin-walled structures. This property is used for plastic collapse. Thin-walled structures are not only good energy absorbers, but also relatively cheap and light in weight. The collapse mechanism in latticed tubes is as follows: first, the cells start closing as the load increases, and a plastic moment is applied about nodal intersections. These plastic deformations gradually spread. The failure mechanism specifically appears as plastic hinges at cell junctions.

The force-displacement response curves show gradual increase in the force, which is a favorable behavior for an energy absorbing system since in these systems damping of the force must be gradual. By observing the failure mode of the expanded metal tube and its deformation configuration, we conclude that the deformation mechanism is layered. (Graciano *et al.* 2009, Graciano *et al.* 2012).

Alghamdi (2001) introduced research conducted during the past four decades on energy absorbers subjected to impact loading. Olabi *et al.* (2007) introduced second general review of metal tubes used as energy absorbers in axial collapse. Jones (2010) compared various energy absorbing systems in terms of the effective factors on energy absorption. Upon studying the energy absorbing capacity of the tubes with various cross sections (circular, rectangular, hexagonal, triangular, pyramidal, and conical), Nia and Hamandani (2010) concluded that tubes with circular cross sections have the highest energy absorbing capacity.

Structural shape plays an important role in optimizing the factors that affect energy absorption. The important function to be considered when developing energy absorbing structures is to reduce the initial force peak in the force-displacement curve response. In applied energy absorber programs, the initial peak force must be reduced for stabilizing the structural response under quasi-static loading. The initial peak force in axial compression tests can be reduced via introducing some kind of defect such as grooves (Zhang *et al.* 2007). Latticed energy absorbers can meet all the requirements for efficient energy absorption. Graciano *et al.* (2012) studied the axial collapse of circular tubes made of expanded metal sheets. Their test results showed that the collapse mechanism depended on cell direction, and that the initial peak force depended on the number of cross sectional cells (Graciano *et al.* 2013).

Impact tests and numerical analysis are concentrated on the failure mechanism as well as the load bearing capacity. On the average, impact loading is applied via free fall of a hammer. Due to the specific features of impact loading, the dynamic response of the structure under impact loading is evidently different from that under quasi-static loading. These results were recorded completely during testing (Qu *et al.* 2014).

Variations of the impacting mass affects only the structural deformation and has no considerable effect on energy-absorption productivity. If a thin-walled part collapses, variations in its thickness would directly affect the structure's cross section. Impact loading increases the thickness of the structure and reduces its deformation, but can fully absorb the impact energy. Thus, wall thickness has a considerable effect on energy absorption. Velocity variation of the

impacting body would directly change the impact force and cause a change in the initial peak force and the mean force as well. Test results show that kinetic energy is affected more by the velocity of the impacting body than by its mass. This also affects the amount of the absorbed energy (Tai *et al.* 2010).

To better understand the behavior of thin-walled structures, these structures were investigated experimentally, analytically, and numerically. The experimental method is perhaps the most expensive method from the viewpoint of time and material selection, but is necessary for validating numerical methods. With due regard of the tests conducted on long and short aluminum tubes, their global and progressive buckling were studies. In short, metal energy absorbers fail under axial compressive loads in various modes including axial collapse, global buckling, or at a point depending on geometric parameters (length and cross sectional area) (Graciano *et al.* 2013). Gupta and Venkatesh (2006) also conducted experimental and numerical studies on cylindrical aluminum sheets with different lengths and diameters. Advances in computational power in the past two decades have prompted researchers to turn to numerical methods for analyzing nonlinear and energy absorbing behaviors of structures (Li *et al.* 2012).

The basic types of Expanded Metal products are standard, flattened, grating, architectural (or decorative) meshes, and fine meshes. These products have thousands of applications for enclosure, protection, support, decoration, and filtration, including grills, fencing, walkways, furniture, etc. The light weight and strength of Expanded Metal make it an ideal material for a wide variety of commercial and industrial security applications. Storefront protectors, stairway and warehouse enclosures, lockers and tool room partitions are among its many uses. Flattened Expanded Metal is manufactured by passing the standard expanded sheet through a cold-roll reducing mill. The result is a smooth, flat and level sheet. Flattened Expanded Metal is used in a variety of specialty applications, such as lawn furniture, book and storage shelves, lamps and lamp shades, fireplace screens, many types of grilles, occasional tables, folding screens, room dividers, and air filtration filters. Standard Expanded Metal as it comes from the press. The strands and bonds are set at a uniform angle to the plane of the sheet. This gives added strength and rigidity, as well as skid-resistant surface (EMMA 2012).

Expanded metal sheets are basically manufactured in two basic types: standard (EMS) and flattened (EMF). These two sheets are quite different in geometry and mechanical properties. The EMF type undergoes additional cold-work, in which the EMS sheet is passed through a cold-roll reducing mill (Smith *et al.* 2014).

In their studies on latticed absorbers, researchers investigated the behavior of the absorbers under static loading. In this study, the behavior of an absorber under impact loading was investigated experimentally and numerically. As experimental tests are time consuming and involve high costs, numerical simulation techniques can be implemented in their stead. The absorbers used in this study were different in terms of the number of their longitudinal cells and cell angles. The purpose of this study was to investigate, both experimentally and numerically, the behavior and type of collapse experienced by the absorbers as a result of increasing the number of their longitudinal cells and, subsequently, comparing the results. All the samples had the same mass and impacting weight velocity.

2. Definitions, principles, and theoretical fundamentals

To investigate the behavior of expanded metal tube absorbers, we first introduce the parameters

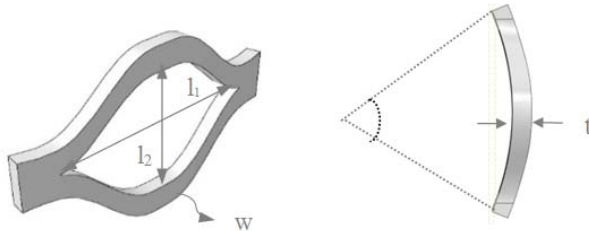


Fig. 1 Expanded metal

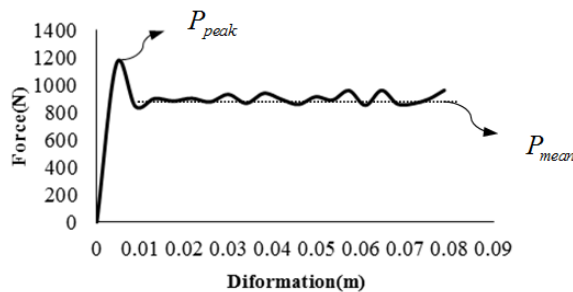


Fig. 2 The description of the peak load and mean crushing force

of these absorbers. Patterns in expanded metal tube absorbers are designated with two parameters, namely, the smaller length (l_2) and the larger length (l_1) (Fig. 1). Two types of collapse were observed in terms of the responses. A specific plastic collapse mode occurred at $\alpha=0$, and for $\alpha=90$ causing global buckling and failure of the structure (Graciano *et al.* 2012).

2.1 The parameters

The initial peak force (P_{peak}), the mean force (P_m), the energy absorption capacity (E_a), and the shape factor (η) are the parameters used for measuring the absorber (Fig. 2). There are other parameters as well, such as the absorbed energy per unit weight (specific energy absorption or SEA). These parameters are very significant in the design system. Weight is used as a limiting factor. The absorbed energy is equal to the area under the force-displacement curve. The shape factor is calculated by dividing the mean force by the initial peak force (Graciano *et al.* 2009) (Eq. (1)-(4)).

$$E_a = \int_{x_2}^{x_1} F(x) dx \quad (1)$$

$$P_m = \frac{E_a}{x_2 - x_1} \quad (2)$$

$$\eta = \frac{P_m}{P_{peak}} \quad (3)$$

$$SEA = \frac{E_a}{W_m} \quad (4)$$

2.2 Strain rate

In transportation industries, design requirements must lead to improved vehicle crashworthiness. For this reason, high strength steels have now replaced weaker steels.

Therefore, it is necessary to better identify structural systems behavior, particularly their energy capacity and the conditions required for better energy absorption by them under impact loads. The sensitivity to strain rate of steel must be considered in structural design. In dynamic loading, strain rate sensitivity of materials is highly important and must be considered in design. The Johnson-Cook or Cowper-Symonds formulas can be used for this purpose (Jones 2010).

2.2.1 The Johnson-Cook theory

In this model, considered as a visco-elastic model, strain rate and temperature are interdependent (Johnson *et al.* 1983). The Johnson-Cook model is suitable for wide-range strain rates and temperature changes where ductility increases due to plastic loss. This model is described as a coefficient of strain, strain rate, and temperature. An increase in the strain rate would lead to increased hardness (Dietenberger *et al.* 2005).

In the Johnson-Cook model, a nonlinear elastic-plastic behavior is assumed for materials. The simplified Johnson-Cook model equation is given Eq. (5) and Eq. (6). This relation is proposed for impact loading where an oscillatory stress-strain diagram is obtained (Zachary *et al.* 2005).

$$\sigma = (A + B\dot{\varepsilon}^n)(1 + C\dot{\varepsilon}_p)(1 - T^{*m}) \quad (5)$$

$$T^* = \frac{T - T_{room}}{T_{melt} - T_{room}} \quad (6)$$

where A is the yield stress, B is the strain hardening factor, n is the strain hardening index, C is the strain rate sensitivity parameter, T^* is the homologous temperature, and m is the thermal softening coefficient. Where T_{room} is the room temperature during the test and T_{melt} represents the known melting temperature of the material (Nicholas *et al.* 1990).

3. Experimental study

In this section, the expanded metal tubes are studied empirically. The tests were conducted for two different cases where the shape of cells and the number of longitudinal cells were changed. The results obtained for cell angles of $\alpha=0$ and $\alpha=90$ degrees are presented in the same order. Loading conditions were the same for both cases, and impact loading was applied. The drop hammer apparatus was used for the tests.

3.1 Test apparatus

In the drop hammer apparatus, a weight is dropped from a specific height, causing the absorber to collapse. The sensors mounted on the apparatus measure the force and collapsed length of the absorber. The accelerometer attached to the impacting weight and connected to a computer (as shown in the Fig. 3) would plot the variations of acceleration with time. Kinetic energy is released as a result of the free fall of the weight.



Fig. 3 Drop hammer apparatus and accelerometer sensors

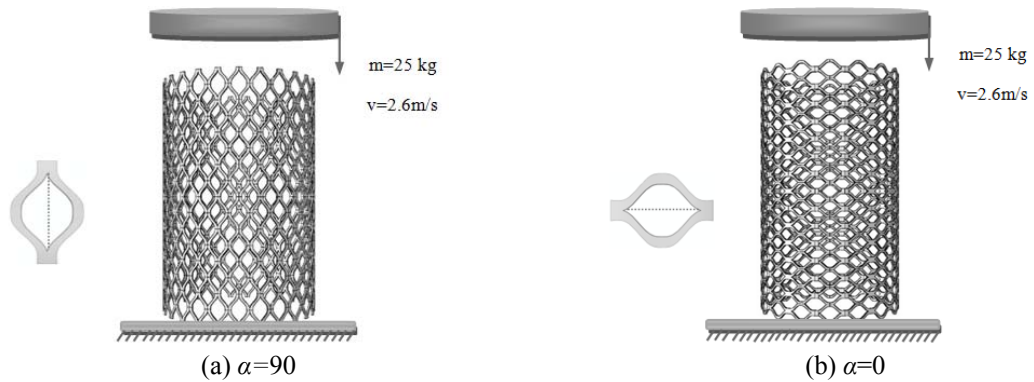


Fig. 4 Models and boundary conditions

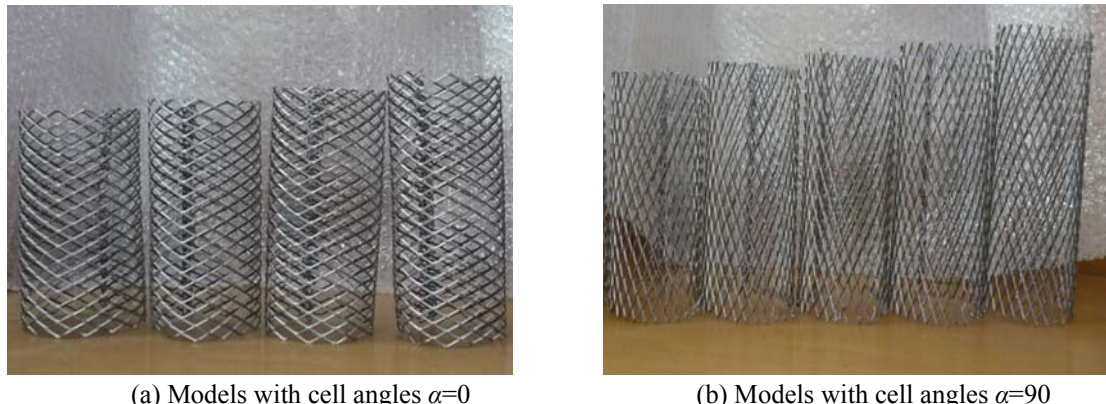


Fig. 5 Experimental models

3.2 Model specifications

Nine models (samples) were prepared. In the following Fig. 4, the models with cell angles of $\alpha=0$ and $\alpha=90$ degrees are shown. The number of cells in these models are different. Materials used in the manufacture of Flattened Expanded Metal include Cold-rolled ASTM A611 (EMMA

2012). The material used was ASTM A-611 of yield strength 553.1 MPa, ultimate strength 705 MPa, Young's modulus 211 MPa, density 7800 kg/m³ and Poisson ratio 0.3.

The cell shown here has the following dimensions: $l_1=1.5$ cm, $l_2=1$ cm, $t=1$ mm (thickness), and $w=2$ mm (width) (Figs. 4-5).

The studied models had cell angles of $\alpha=0$ and $\alpha=90$ degrees and different cell numbers. The specifications of these models are given in the following table (W_m is the mass of the models).

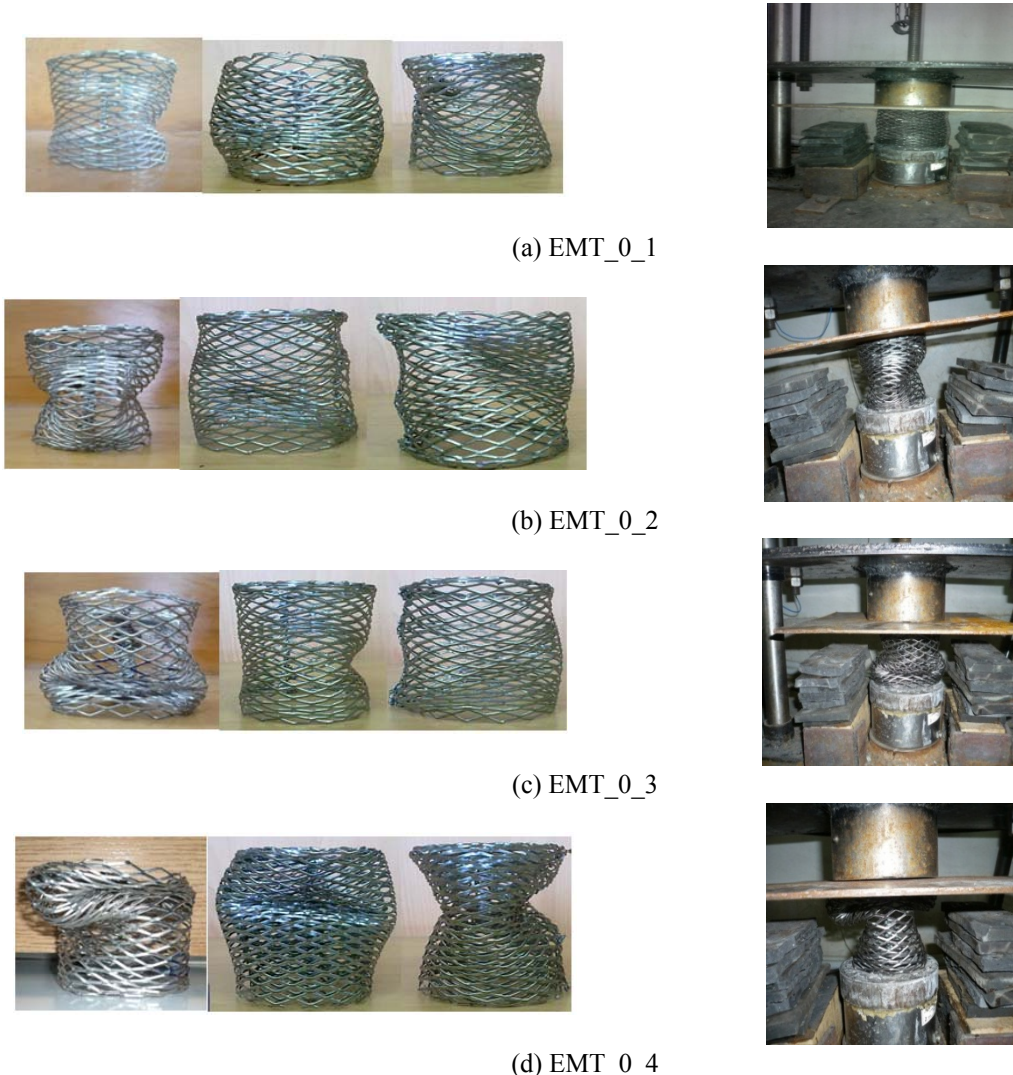
In Table 1, the experimental tests of specimens with angle 0 are performed. A total of 12 tests were performed, for each geometry three tests were conducted in order to check the repeatability of the results. In Table 2, the experimental tests of specimens with angle 90 are performed. A total of 15 tests were performed, for each geometry three tests were conducted in order to check the repeatability of the results.

Table 1 Specifications of models with cell angles $\alpha=0$

Models	α	N_C	N_L	D (cm)	L (cm)	t (mm)	v (m/s)	m (kg)	W_m (gr)
EMT_0_1_1	0	15	15	10	16.5	1	2.6	25	110
EMT_0_1_2	0	15	15	10.1	16.45	1	2.6	25	112
EMT_0_1_3	0	15	15	10.12	16.55	1	2.6	25	111
EMT_0_2_1	0	15	16	10	17.7	1	2.6	25	120
EMT_0_2_2	0	15	16	10.11	17.72	1	2.6	25	121
EMT_0_2_3	0	15	16	10.15	17.69	1	2.6	25	121
EMT_0_3_1	0	15	17	10	18.5	1	2.6	25	130
EMT_0_3_2	0	15	17	10.11	18.51	1	2.6	25	132
EMT_0_3_3	0	15	17	10.11	18.48	1	2.6	25	128
EMT_0_4_1	0	15	18	10	19.5	1	2.6	25	140
EMT_0_4_2	0	15	18	9.96	19.46	1	2.6	25	137
EMT_0_4_3	0	15	18	10.1	19.52	1	2.6	25	141

Table 2 Specifications of models with cell angles $\alpha=90$

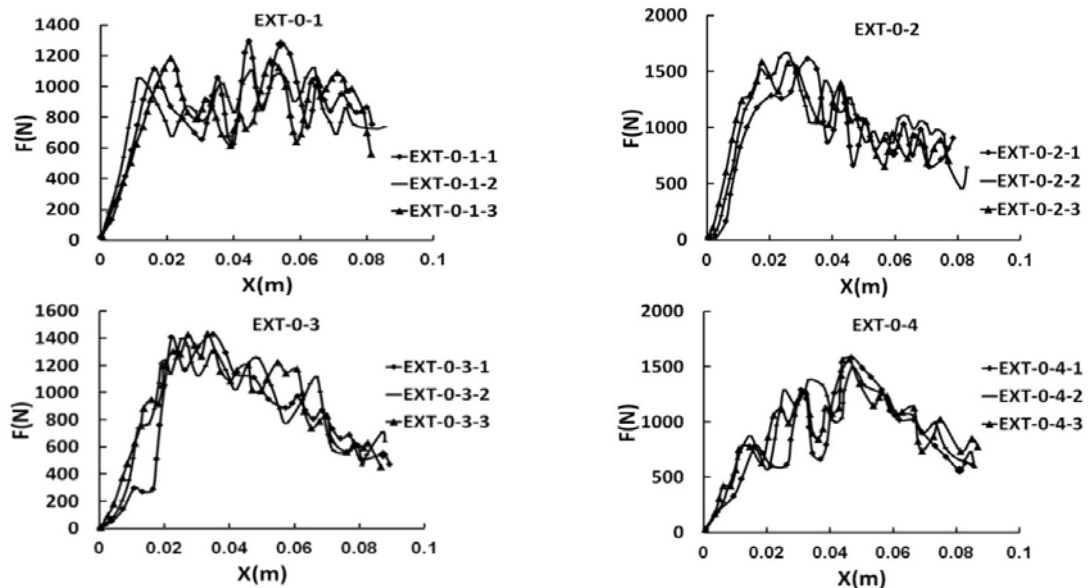
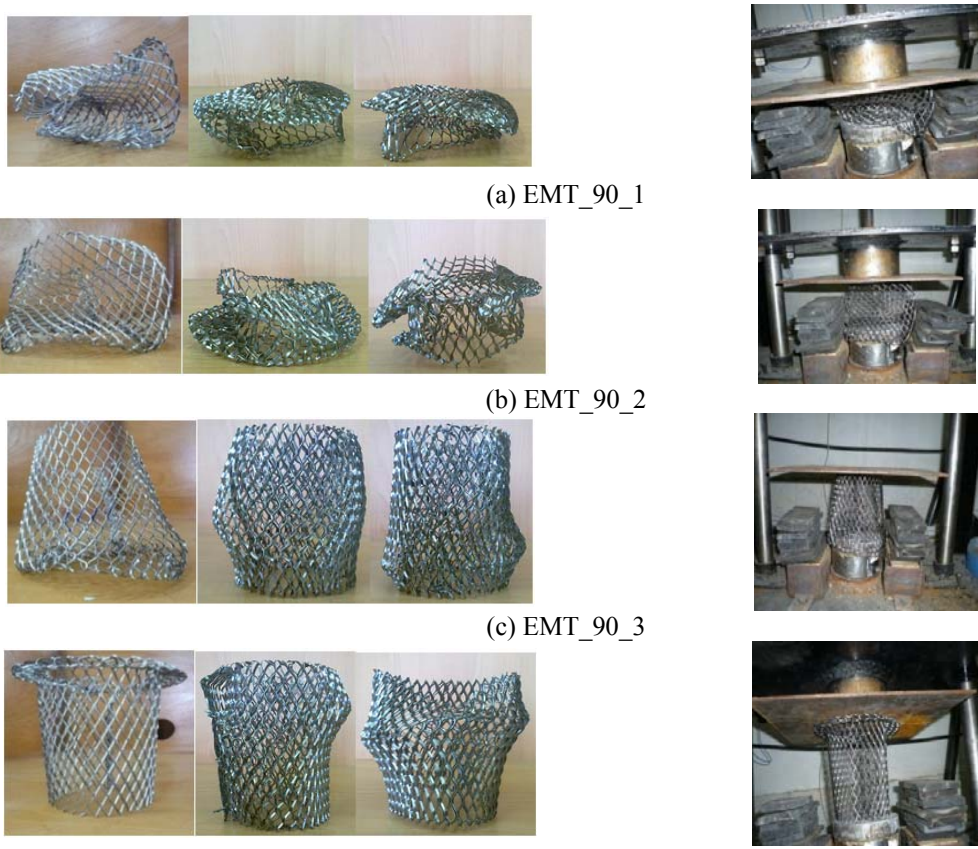
Models	α	N_C	N_L	D (cm)	L (cm)	t (mm)	v (m/s)	m (kg)	W_m (gr)
EMT_90_1_1	90	26	8.5	10	17.5	1	2.6	25	120
EMT_90_1_2	90	26	8.5	10.04	17.47	1	2.6	25	119
EMT_90_1_3	90	26	8.5	10.03	17.51	1	2.6	25	122
EMT_90_2_1	90	26	9	10	18.5	1	2.6	25	130
EMT_90_2_2	90	26	9	9.98	18.55	1	2.6	25	128
EMT_90_2_3	90	26	9	10.02	18.53	1	2.6	25	133
EMT_90_3_1	90	26	9.5	10	19.5	1	2.6	25	140
EMT_90_3_2	90	26	9.5	10.05	19.52	1	2.6	25	137
EMT_90_3_3	90	26	9.5	10.06	19.47	1	2.6	25	142
EMT_90_4_1	90	26	10	10	20.5	1	2.6	25	150
EMT_90_4_2	90	26	10	10.02	20.42	1	2.6	25	145
EMT_90_4_3	90	26	10	9.91	20.55	1	2.6	25	152
EMT_90_5_1	90	26	10.5	10	21.5	1	2.6	25	160
EMT_90_5_2	90	26	10.5	9.92	21.54	1	2.6	25	153
EMT_90_5_3	90	26	10.5	10.04	21.42	1	2.6	25	164

Fig. 6 Collapse of models with cell angle $\alpha=0$

3.3 Experimental results and discussion

The expanded metal tubes used as energy absorbers are easily available and their price is reasonable. To investigate these absorbers empirically and test their efficiency in practice, we subjected them to certain experimental tests. In Fig. 6 and Fig. 7, the experimental tests of specimens with angle 0 are performed. A total of 12 tests were performed, for each geometry three tests were conducted in order to check the repeatability of the results. In Fig. 8 and Fig. 9, the experimental tests of specimens with angle 90 are performed. A total of 15 tests were performed, for each geometry three tests were conducted in order to check the repeatability of the results.

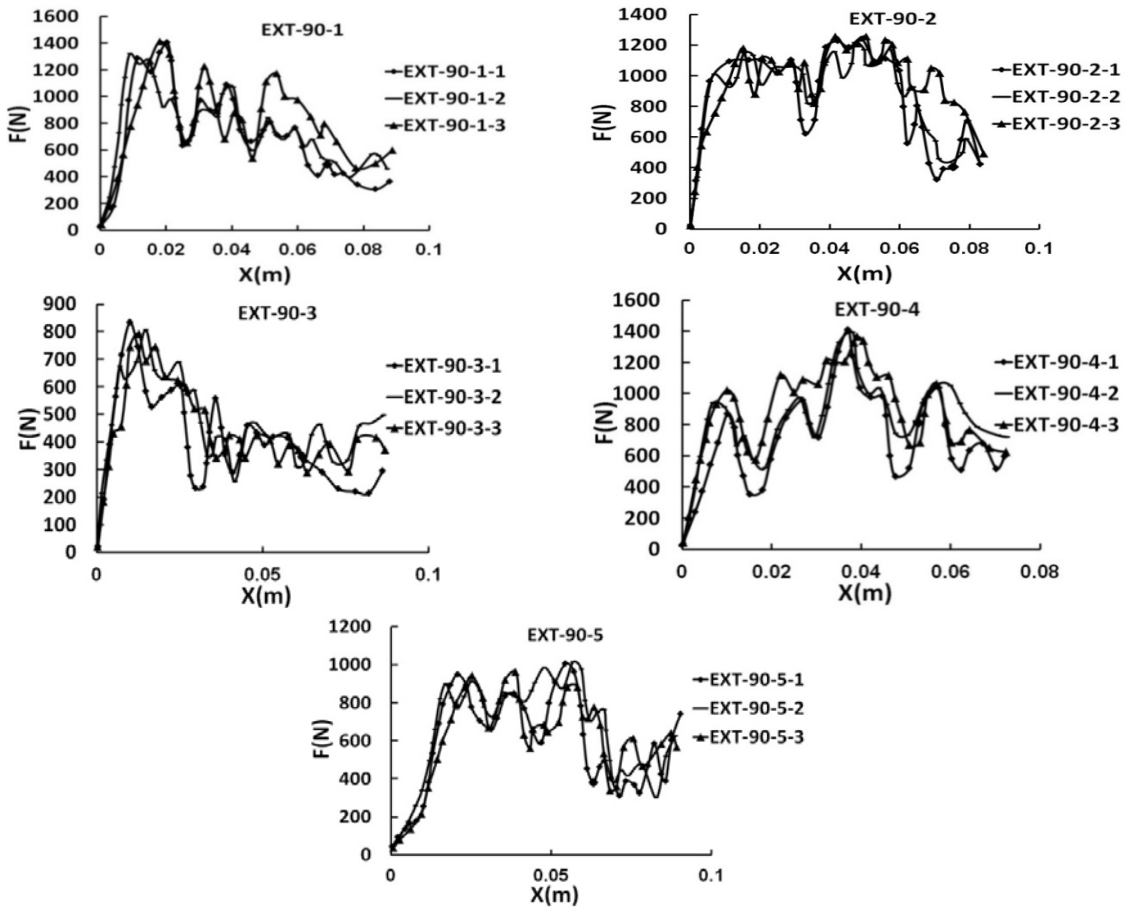
Two types of absorber were tested under identical conditions: absorbers with $\alpha=0$ cell angles and those having $\alpha=90$ cell angles. Due attention to experimental results and observations showed

Fig. 7 Force-displacement diagrams of models with cell angle $\alpha=0$ Fig. 8 Collapse of models with cell angle $\alpha=90$



(e) EMT_90_5

Fig. 8 Continued

Fig. 9 Force-displacement diagrams of models with cell angle $\alpha=90^\circ$

that the absorbers with $\alpha=0$ collapsed symmetrically and cells closed onto one another after collapsing, thus exhibiting an efficient collapse mechanism Fig. 10.

In some models, point buckling was observed which was attributed to the existing faults in these models. Also, the force-displacement diagrams for these models showed relatively regular oscillations (Fig. 11). The data obtained from these diagrams showed that the initial force peak was favorable and close to the mean force. This is also reflected in the calculation of the shape factor. The energy absorbing capacity was calculated for all the models (Tables 3-4) and (Fig. 12).



Fig. 10 Symmetric collapsed

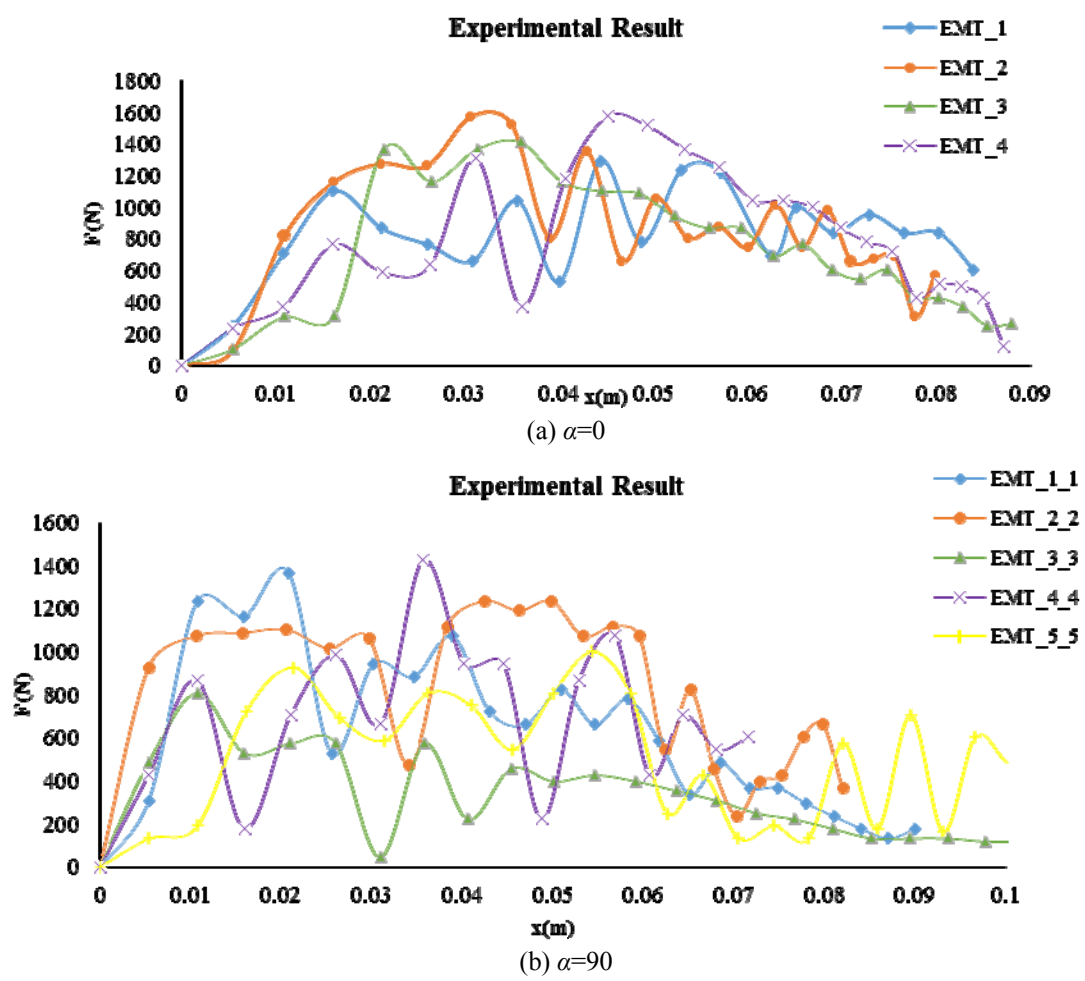


Fig. 11 Force-displacement diagrams

All the models exhibited more or less equal energy absorption, but are different in terms of the collapse to the initial length ratio. This is indicative of the high efficiency of these models. The absorbers with $\alpha=90$ degrees buckled due to their longitudinal strength. The tests showed that all the samples underwent global buckling. Buckling leads to insufficient energy absorption and does

Table 3 Experimental results of models with cell angle $\alpha=0$

models	Peak force P (N)	Mean force P_m (N)	Collapse length δ (m)	Energy absorbed E (J)	Impact energy E_{ie} (J)	Percent of collapse δ/L	Shape factor η	SEA (J/gr)
EMT_0_1	1103.438	826.2	0.083884	69.3	84.5	51%	0.75	0.63
EMT_0_2	1280	909	0.079749	72.5	84.5	45.6%	0.71	0.6
EMT_0_3	1368	760	0.087919	66.8	84.5	47.5%	0.6	0.52
EMT_0_4	1309.413	809.8	0.087183	70.6	84.5	44.8%	0.62	0.5

Table 4 Experimental results of models with cell angle $\alpha=90$

models	Peak force P (N)	Mean force P_m (N)	Collapse length δ (m)	Energy absorbed E (J)	Impact energy E_{ie} (J)	Percent of collapse δ/L	Shape factor η	SEA (J/gr)
EMT_90_1	1235.85	661.3	0.089978	59.9	84.5	48.7%	0.54	0.49
EMT_90_2	1074.013	865	0.81971	71.9	84.5	42%	0.8	0.55
EMT_90_3	809.1879	330	0.097784	32.2	84.5	47.7%	0.4	0.23
EMT_90_4	868.0375	700.3	0.071541	50.1	84.5	33.3%	0.8	0.334
EMT_90_5	926.8875	527.7	0.096654	51	84.5	43%	0.57	0.32

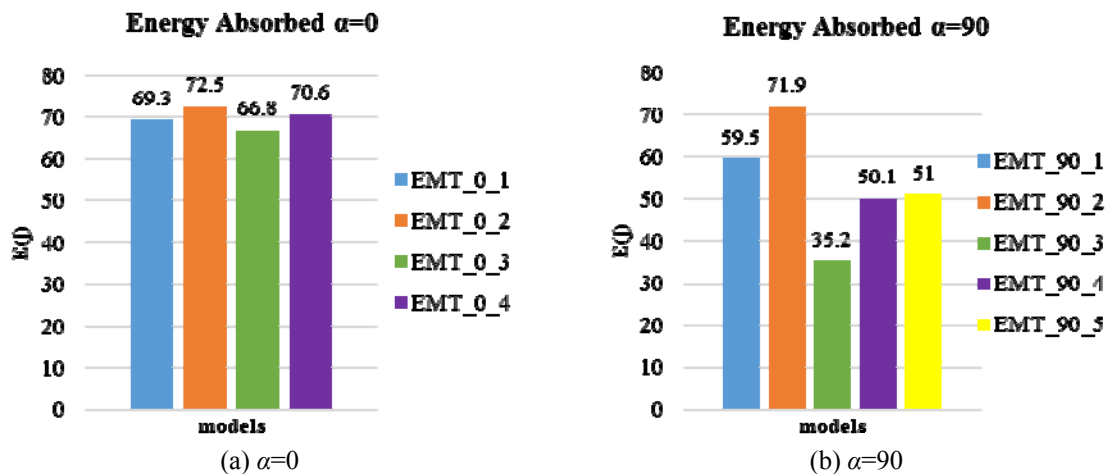


Fig. 12 Experimental study for energy absorbed

not provide proper force peak and mean force values for these absorbers. Also, according to the tests, the absorbers with $\alpha=0$, and length to diameter ratios of less than 2.15 would not buckle.

4. Numerical study

The ABACUS computer program was used to investigate the energy absorbing capacity in expanded metal tube cylindrical absorbers. ABACUS is a finite element package widely used in mechanical applications for solving linear, nonlinear, static, dynamic, impact, etc. problems. (ABAQUS user manual 2010)

In this section, we investigate the effect of height parameter and the number of absorber longitudinal cells on energy absorption, peak force, and the collapsed length. The simulation method and application of loading conditions are fully explained.

4.1 Finite element model

For developing an expanded metal tube absorber, we first design a cell as in the following figure 12. By putting together several such cells, an expanded metal tube absorber is created. The cell shown here has the following dimensions: $L_1=1.5$ cm, $L_2=1$ cm, $t=1$ mm (thickness), and $w=2$ mm (width) (Fig. 13).

The structured meshing method was used in this study. The elements were three dimensional and hex-dominated (C3D8R). Each element was 1 mm long. The meshing method is shown in the following Fig. 13.

4.2 Absorber material

Materials used in the manufacture of Flattened Expanded Metal include Cold-rolled (ASTM A611) (EMMA, 2012). The material characteristics and stress-strain diagram for this steel are given in Table 5 and Fig. 14.

Dynamic loading is applied where material strain rate must be considered. Here, the Johnson-Cook model was used. The coefficients for this model are given in the Table 6.

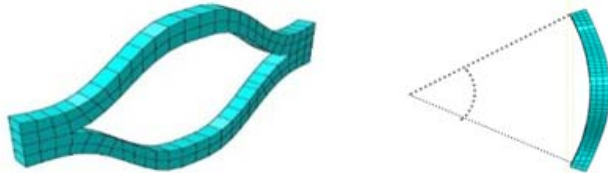


Fig. 13 Meshing method

Table 5 Material properties for steel

σ_y (MPa)	σ_u (MPa)	E (GPa)	ϑ	ρ (kg/m ³)
553.1	705	211	0.3	7800

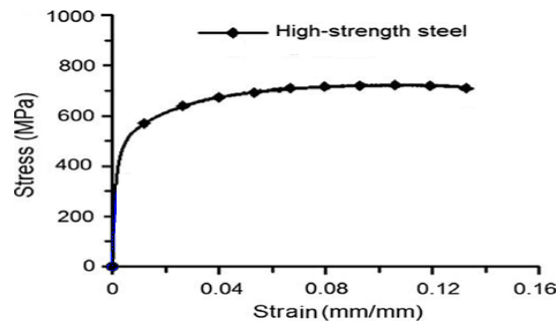


Fig. 14 stress-strain diagram (Tai *et al.* 2010)

Table 6 Johnson-Cook coefficients for steel ASTM A611 (ANSI 1979)

<i>A</i> (MPa)	<i>B</i> (MPa)	<i>C</i>	<i>n</i>	<i>m</i>	<i>T_m</i> °C
553.1	600.8	0.0134	0.234	1	1460

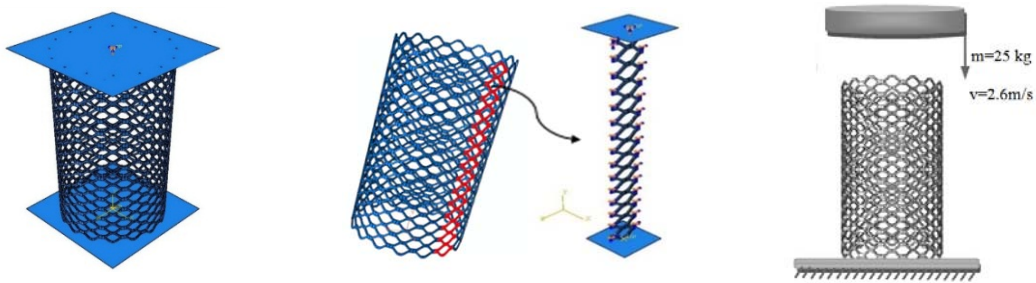


Fig. 15 Schematic of column and boundary condition

Table 7 The specimen geometry and test detail

Models	α	N_C	N_L	D (cm)	L (cm)	t (mm)	v (m/s)	m (kg)
EMT_0_1	0	15	15	10	16.5	1	2.6	25
EMT_0_2	0	15	16	10	17.5	1	2.6	25
EMT_0_3	0	15	17	10	18.5	1	2.6	25
EMT_0_4	0	15	18	10	19.5	1	2.6	25
EMT_0_5	0	15	19	10	20.5	1	2.6	25
EMT_0_6	0	15	20	10	21.5	1	2.6	25

4.3 Type of loading and boundary conditions

In the simulation, an impact load is applied via free fall of an impacting body. The absorber is placed between two rigid plates. The lower plate is fixed and the 25 kg upper plate moves downward at a speed of 2.6 m/s. The computation time is 0.034 seconds (Fig. 15).

Since the absorber is symmetrical, only one of the 15 absorber columns need to be simulated so as to reduce computation time. Upon applying the load on the one column, the values of the initial force peak and absorbed energy are obtained and the results multiplied by 15. As the absorber collapses, the cells come in contact with one another, so a coefficient of friction of 0.2 is assumed.

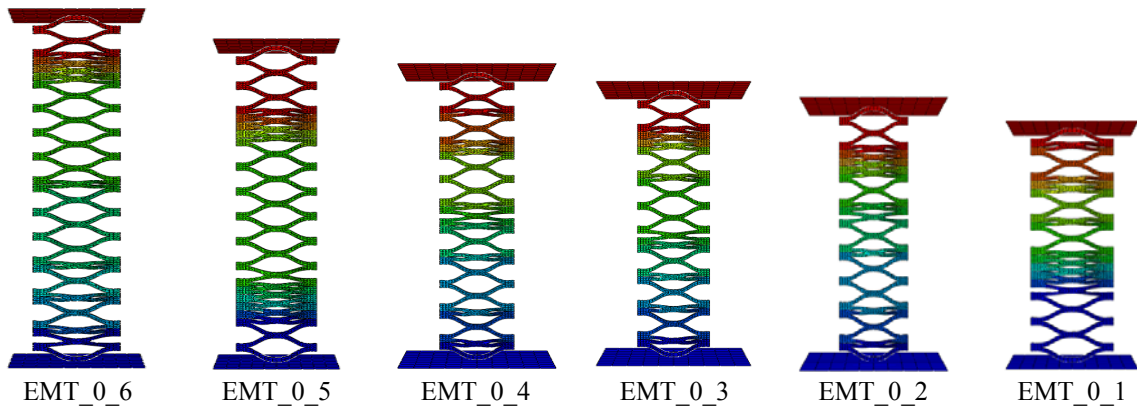


Fig. 16 Type of models collapse

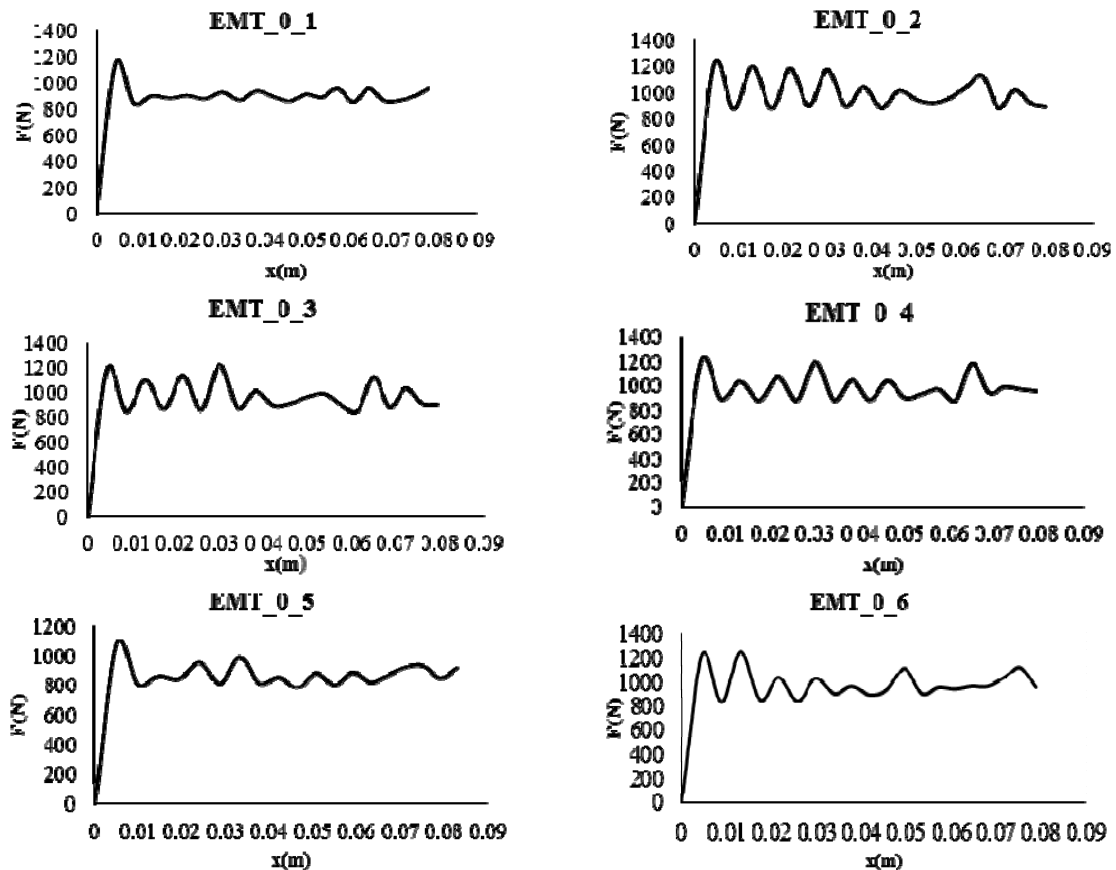


Fig. 17 Force-displacement diagrams of models

4.4 Models

The models were studied for $\alpha=0$ and variable number of cells. The boundary conditions and

type of loading were the same for all the models. Specifications of the models are given in the following table. In this table, EMT (expanded metal tubes) represents the model name, α is cell angle, N_C is the number of circular cells, N_L is the number of longitudinal cells, D is model diameter, L is length, t is wall thickness, m is mass, and v is impact velocity (Table 7).

4.5 Numerical result and discussion

The results obtained from numerical simulation are discussed below. As was said before, the efficiency of energy absorbers is measured from the Force-displacement diagram, and the area under this curve is equal to the absorbed energy. In the following discussion, all the absorbers have a zero cell angle ($\alpha=0$) and their respective force-displacement diagrams and type of collapse are presented (Figs. 16-17).

All the force-displacement diagrams are given in the Fig. 18.

As seen in this figure, the variations in the diagrams and the initial force peak are closely similar for all the absorbers. The area under the force-displacement curve equals the absorbed energy, so by integrating this function, the absorbed energy can be obtained. These results are presented below.

Throwing an impacting body would transfer kinetic energy. The total kinetic energy produced due to the impacting body is obtained from the Eq. (7) (impact energy).

$$E_{ie} = \frac{1}{2}mv^2 \quad (7)$$

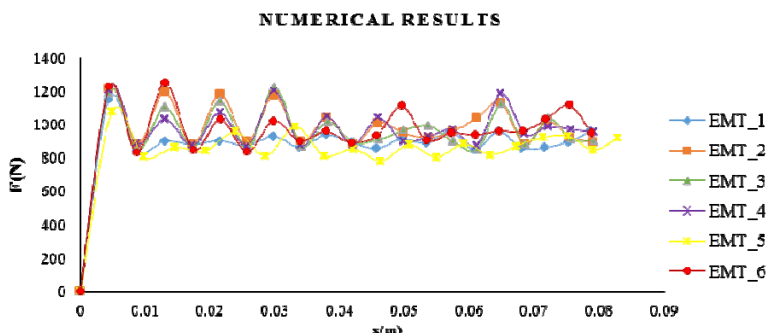


Fig. 18 Force-displacement diagrams

Table 8 Numerical results

Models	Peak force P (N)	Mean force P_m (N)	Collapse length δ (m)	Energy absorbed E (J)	Impact energy E_{ie} (J)	Percent of collapse δ/L	Shape factor η
EMT_0_1	1151.048	889.74	0.078679	70	84.5	48%	0.78
EMT_0_2	1216.547	977	0.079011	77.2	84.5	45.2%	0.8
EMT_0_3	1188.051	950.6	0.079211	75.3	84.5	43%	0.8
EMT_0_4	1209.488	960.17	0.079152	76	84.5	41%	0.8
EMT_0_5	1078.483	853	0.082913	70.7	84.5	40.5%	0.8
EMT_0_6	1224.886	957.6	0.078841	75.5	84.5	39%	0.78

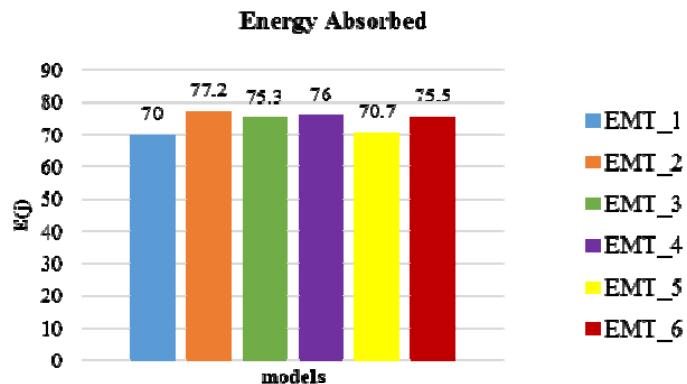


Fig. 19 Numerical study for energy absorbed

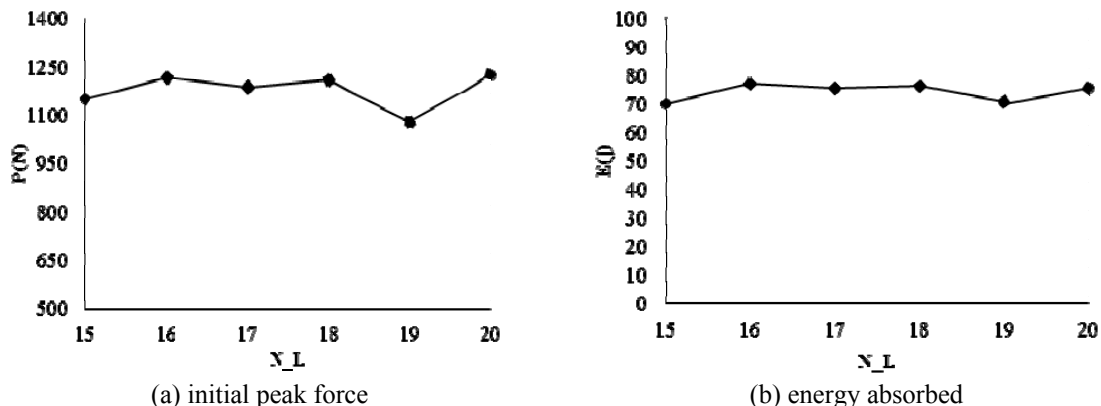


Fig. 20 Effect of longitudinal cells on initial peak force and energy absorbed

The mean force is calculated as the energy absorbed divided by the collapsed length (Table 8 and Fig. 19).

These results showed that the absorber collapse was symmetrical, thus producing a stable force-displacement diagram. Due to the applied axial load, the cells collapse onto one another, thus absorbing the impact energy. An important parameter in energy absorbers is shape factor or collapse force efficiency. The nearer the shape factor to unity, the more efficient the absorber and the more stable the collapse would be. The values of shape factor were calculated for all the models. As can be seen in the table of results, these shape factors are close to unity, indicating that the values of the mean force and the initial force peak are close. As a result, a uniform force-displacement diagram as well as a greater energy absorption capacity can be obtained (Fig. 20).

5. Experimental vs. numerical results

In this section, the results obtained from numerical simulation are compared with those obtained from tests. First, a numerical study was conducted on the absorbers with $\alpha=0$, and then the corresponding results for the absorbed energy, the initial force peak, the mean force, and other

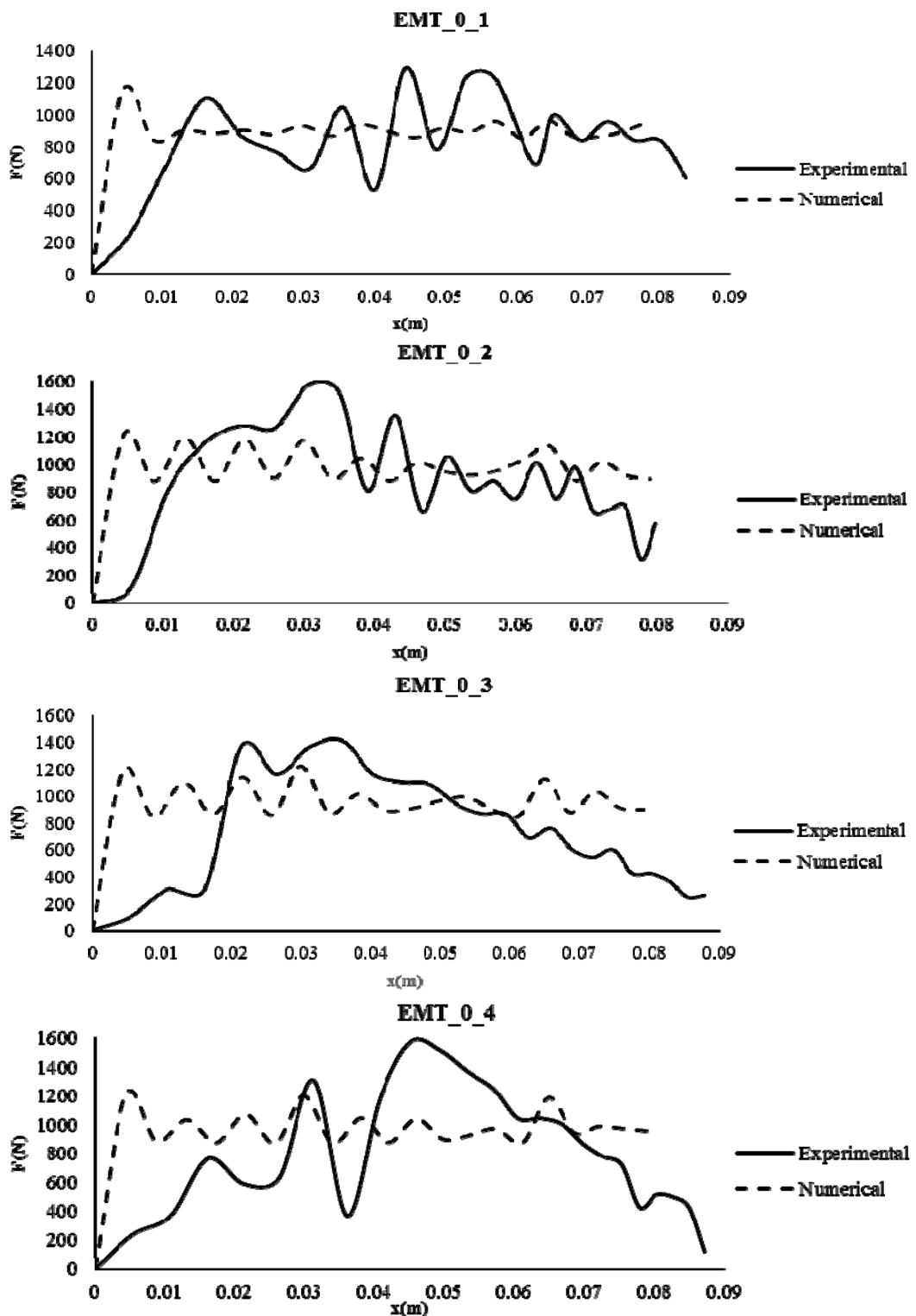
Fig. 21 Experimental vs. numerical force- displacement diagrams for $\alpha=0$

Table 9 Experimental vs. numerical for initial peak force

models	initial peak force P (N)		error e (%)
	Experimental	Numerical	
EMT_0_1	1103.438	1151.048	4.32%
EMT_0_2	1280	1216.547	4.95%
EMT_0_3	1368	1188.051	13.15%
EMT_0_4	1309.413	1209.488	7.63%

Table 10 Experimental vs. numerical for mean force

models	initial peak force P (N)		error e (%)
	Experimental	Numerical	
EMT_0_1	826.2	889.74	7.69%
EMT_0_2	909	977	7.48%
EMT_0_3	760	950.6	25.07%
EMT_0_4	809.8	960.17	18.57%

Table 11 Experimental vs. numerical for energy absorbed

models	initial peak force P (N)		error e (%)
	Experimental	Numerical	
EMT_0_1	69.3	70	7.69%
EMT_0_2	72.5	77.5	7.48%
EMT_0_3	66.8	75.5	25.07%
EMT_0_4	70.6	76	18.57%

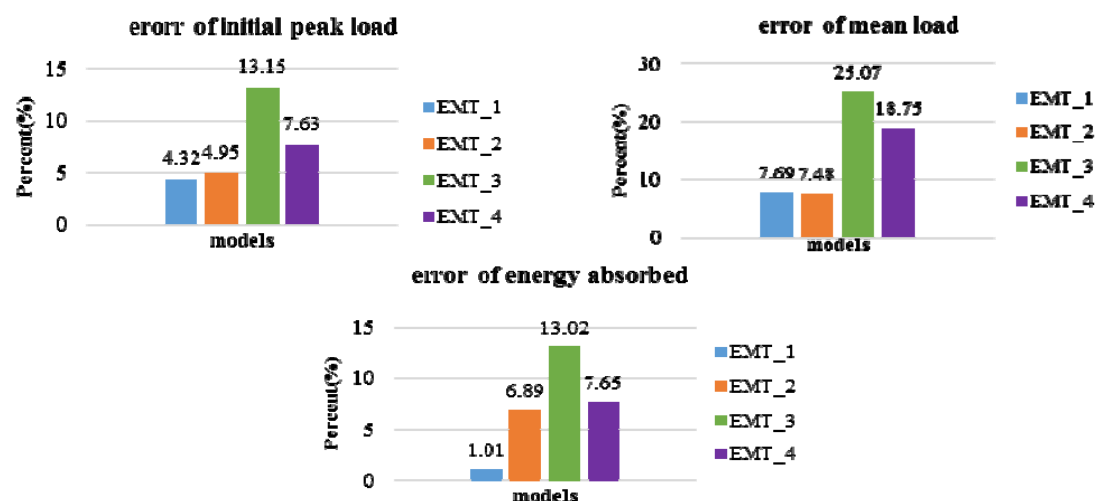


Fig. 22 Error of experimental vs. numerical

parameters were compared. Then, these absorbers were studied empirically. As mentioned before, the absorbers with $\alpha=0$ were much more efficient than those with $\alpha=90$ degrees. Therefore, the simulation and experimental results obtained for the former $\alpha=0$ absorbers shall be compared here.

5.1 Results and discussion

In this section, the force-displacement diagrams obtained from numerical simulation and tests were compared (Fig. 21). As can be seen, the diagrams are relatively similar. The absorbed energy, the initial force peak and the mean force obtained via tests and the simulation are compared and the results presented in Tables 9-11 and Fig. 22.

In this section, the results obtained from tests are compared with those obtained from numerical simulation. Since experiments are time consuming and expensive, numerical simulation can be conducted in their stead. As observed from the results, the force-displacement diagrams obtained from simulation are in good agreement with those obtained from the tests. Other important parameters, namely, the initial force peak, the mean force, and the absorbed energy were compared for the two methods (tests vs. simulation) as well. The obtained results showed relative agreement and some cases errors were detected.

6. Conclusions

- Due to their structural form, expanded metal tubes exhibit a symmetrical collapse mechanism. This leads to a regular force-displacement diagram. Also, the initial force peak in these absorbers is not considerable and is closer to the mean force. The calculated shape factor or collapse force efficiency also points out the same conclusion. The calculated shape factors show that expanded metal tubes have a high energy absorbing efficiency.

- Increasing the number of cells did not considerably affect the initial force peak or the mean force. Collapsing of the cells dissipate energy. Therefore, by increasing the number of cells, the energy absorption capacity can be increased.

- Increasing cell angles had a considerable effect on the behavior of the absorbers. It was observed that those absorbers with cell angles of $\alpha=0$ had symmetrical collapse as well as a continuous force-displacement diagram. Also, these absorbers exhibited very favorable initial force peak and energy absorbing capacity values. On the other hand, the absorbers with $\alpha=90$ all underwent buckling and their force-displacement diagrams were not continuous. Their energy absorption was not favorable either. Therefore, we can conclude that the expanded metal tubes with $\alpha=0$ are much more efficient and energy absorbent.

- An important parameter in energy absorbers is the specific energy absorption (SEA) or energy absorption efficiency. This parameter is obtained by dividing the energy absorbed by the absorber by the absorber mass. Expanded metal tubes are lightweight and can absorb high amounts of energy. Therefore, we conclude that this type of absorber has a high efficiency. It was also observed that upon increasing the shape factor or collapse force efficiency, the SEA shall also increase.

- Buckling is of particular significance in energy absorbers. If the absorber undergoes buckling due to axial loading, it experiences unsymmetrical collapse and its energy absorbing capacity is reduced. This must be taken into account when designing absorbers. The tests showed that in absorbers with $\alpha=0$ (cell angle), if the absorber's length to diameter ratio is less than 2.15, then buckling will not occur.

- The results obtained from numerical simulation and the conducted tests showed good agreement between the corresponding values obtained for the energy absorbed, the initial force peak, the mean force, and the force-displacement diagram. Therefore, the numerical model can

well replace tests in the design process for this type of absorber.

References

- ABAQUS Analysis User's Manual (2010), v6.10 Section 6.3.3, Explicit Dynamic Analysis.
- Alghamdi, A.A.A. (2001), "Collapsible impact energy absorbers: an overview", *Thin Wall. Struct.*, **39**, 189-213.
- ANSI/ASTM A611-72 (1979), Standard Specification for STEEL, COLD-ROLLED SHEET, CARBON, STRUCTURAL.
- Dietenberger, M., Buyuk, M. and Kan, C.D. (2005), "Development of high strain-rate dependent vehicle model", FHWA/NHTSA National crash Analysis Center.
- EMMA (Expanded Metal Manufacturers Association) (2012), Division of the National Association of Architectural Metal Manufacturers (NAAM), EMMA 557-12: Standards for Expanded Metal.
- Ghamarian, A., Zarei, H.R. and Abadi, M.T. (2011), "Experimental and Numerical Crashworthiness Investigation of Empty and Foam-filled End-capped Conical Tubes", *Thin Wall. Struct.*, **49**(10), 1312-1319.
- Graciano, C., Martínez, G. and Smith, D. (2009), "Experimental investigation on the axial collapse of expanded metal tubes", *Thin Wall. Struct.*, **47**, 953-961.
- Graciano, C., Martínez, G. and Gutiérrez, A. (2012), "Failure mechanism of expanded metal tubes under axial crushing", *Thin Wall. Struct.*, **51**, 20-24.
- Gupta, N.K. and Venkatesh. (2006), "A study of the influence of diameter and wall thickness of cylindrical tubes on their axial collapse", *Thin Wall. Struct.*, **44**, 290-300.
- Huang, M.Y., Tai, Y.S. and Hu, H.T. (2010), "Dynamic crushing characteristics of high strength steel cylinders with elliptical geometric discontinuities", *Theo. Appl. Fract. Mech.*, **54**, 44-53.
- Johnson, G.R. and Cook, W.H. (1983), "A constitutive model and data for metals subjected to large strains, high strain rates and high temperatures", *Proceedings of the 7th International Symposium on Ballistics*, Hague, Netherlands.
- Jones, N. (2010), "Dynamic energy absorption and perforation of ductile structures", *Int. J. Press. Vess. Pip.*, **87**, 482-492.
- Jones, N. (2010), "Energy-absorbing effectiveness factor", *Int. J. Impact Eng.*, **37**, 754-765.
- Li, Z., Yu, J. and Guo, L. (2012), "Deformation and energy absorption of aluminum foam-filled tubes subjected to oblique loading", *Int. J. Mech. Sci.*, **54**, 48-56.
- Martínez, G., Graciano, C. and Teixeira, P. (2013), "Energy absorption of axially crushed expanded metal tubes", *Thin Wall. Struct.*, **71**, 134-146.
- Nia, A.A. and Hamedani, J.H. (2010), "Comparative analysis of energy absorption and deformations of thin walled tubes with various section geometries", *Thin Wall. Struct.*, **48**, 946-954.
- Olabi, A.G., Morris, E. and Hashmi, M.S.J. (2007), "Metallic tube type energy absorbers a synopsis", *Thin Wall. Struct.*, **45**(7-8), 706-726.
- Qu, H., Huo, J., Xu, C. and Fu, F. (2014), "Numerical studies on dynamic behavior of tubular T-joint subjected to impact loading", *Int. J. Impact Eng.*, **67**, 12-26.
- Smith, D., Graciano, C., Martínez, G. and Teixeira, P. (2014), "Axial crushing of flattened expanded metal tubes", *Thin Wall. Struct.*, **85**, 42-49.
- Song, J., Chen, Y. and Lu, G. (2013), "Light-Weight thin-walled structures with patterned windows under axial crushing", *Int. J. Mech. Sci.*, **66**, 239-248.
- Tai, Y.S., Huang, M.Y. and Hu, H.T. (2010), "Axial compression and energy absorption characteristics of high-strength thin-walled cylinders under impact load", *Theo. Appl. Fract. Mech.*, **53**, 1-8.
- Theodore, N. and Recht, R.F. (1990), *High Velocity Impact Dynamics, Chapter 1 Introduction to Impact Phenomena*, John Wiley and Sons, New York, NY.
- Zachary, A. and Ensign, K. (2005), *Determination of the Constitutive Equations for 1080 Steel and*

Vascomax 300, Air force institute of technology, Air Force Univercity.
Zhang, X., Cheng, G., You, Z. and Zhang, H. (2007), "Energy absorption of axially compressed thin-walled square tubes with patterns", *Thin Wall. Struct.*, **45**(9), 737-746.

CC